Research on the calibration method of precipitation micro-physical characteristics sensor

SHU Xiaojian, GAO Taichang*, LIU Xichuan, HU Shuai

(*College of Meteorology and Oceanography, PLA University of Science and Technology, Nanjing* 211101, *China*)

Abstract: In order to diminish the effect of the ambient light and CCD pixel non-uniformity to the Precipitation Micro-physical Characteristics Sensor, a modified calibration scheme was designed and calibration experiments in sunny, cloudy, night, different location of sample space were carried out. Firstly, the characteristics of particle images which affected by ambient light and different location of sample space were analyzed. Secondly, the relevance between particle image features and parameters of image processing were discussed. Finally, the parameter setting scheme were determined, the radium of median filtering algorithm is 3 pixels, the defocusing radius of point spread function(PSF) is 7 pixels, the radium of erosion is 3 pixels, and the binary threshold is obtained from the *Area -thresh* relationship. The results show that the new scheme could deal with the image calibration well, the average errors of equivolumetric diameter was 0.041mm with standard deviation of 0.115mm, and the average errors of the axis ratio was 0.011 with standard deviation of 0.085. The new scheme works well in the field observation too, the observed axis ratio is consistent with the empirical relationship that proposed by Beard. The relative error of accumulation precipitation is -3.06% after calibration, which is improved 1.94% lower than the initial one without calibration.

Key words: precipitation micro-physical characteristics sensor; calibration scheme; particle image features; threshold

1 Introduction

Precipitation is one of the main processes of the water cycle, which is the interaction result of many atmospheric factors, such as dynamics, thermal, vapour. The raindrop shape, size and fall velocity are important parameters in many environmental fields [1] such as investigation on cloud/precipitation microphysical processes, microwave attenuation processes, weather radar applications and weather modification estimation. At present, the vibratory and optical methods are primarily used in precipitation microphysical characteristics measurement. For instance, the Joss-Waldvogel [2] disdrometer infers the size of each raindrop based on the measured impact kinetic energy of raindrops, the OTT Parsivel [3] and Thies [4] distrometers measure the size of particles according to the light signal by extinction. But the former cannot measure the velocity and shape of raindrops, and the latter estimate the vertical size and fall velocity based on the empirical assumption of raindrop shape. The Two-Dimensional Video Disdrometer [5] uses two scan cameras to obtain perpendicular projections of a droplet falling through two parallel sheets of white light, which perhaps is the best device to measure raindrop shape and velocity. However, the 2DVD drop shape measurement can be affected by wind which makes the droplet exist moving in the horizontal direction. The Rain Imaging System [6] uses a charge-coupled device (CCD) image sensor to measure the raindrop shape, but it cannot measure the fall velocity.

In order to improve the precipitation microphysical characteristics measurement ability, the precipitation research team of PLA University of Science and Technology have designed Precipitation Microphysical Characteristics Sensor (PMCS) [7] in 2013. Several rainfall events[8,9] have been observed in 2013 and 2014, which evaluated the instrument's ability of measuring the shape, size, orientation, and fall velocity of naturally hydrometeors, and we discovered that the instrument is still affected by the external environment [10]. Hence, a new calibration

scheme should be carried out. For traditional calibration methods, the output diameter of rain drops is determined by a fixed calibration relationship between the instrument output and the known diameter, however the calibration relationship might be changed by the external factors, such as the ambient light [11], CCD pixel non-uniformity [12], the divergence of parallel light beam etc, which might lead to notable errors in the size measurement of raindrops. Therefore, it is necessary to design a new calibration method to include different measurement circumstances.

In the following sections contain descriptions of the PMCS instrument, the designed processing of calibration scheme and field experiments. The last part summarizes the features of calibration method and the future work of PMCS.

2 The descriptions of PMCS

The PMCS is also known as planar array CCD Drop Size Disdrometer, which consists of four units: optical unit, imaging unit, acquisition and control unit, and data processing unit, as shown in Fig. 1. The optical unit contains a concentration lens, expanded beam lens, and a multi-mode fibre cluster, which provide a parallel and stable light beam for imaging unit. The imaging unit contains one CCD monochrome image sensor and matching driving circuit, which precisely control the exposure for the hydrometeors within the sampling space. The acquisition and control unit contains a digital signal processor (DSP), reset circuit, storage chips, clock circuit, a complex programmable logic device (CPLD), and other support integrated circuits, which achieve quickly acquiring, transmitting and disposing the maximum imaging data in real time. The data processing unit is composed of a PC terminal with relevant utility software, which achieve dealing the imaging data and extracting the precipitation microphysical characteristics.

The PMCS utilize the parallel light beam as imaging background field. When a hydrometeor falling through the sampling space, PMCS could expose this particle twice in one frame image, through precisely controlling the optical and shutter. It can use the images to extract the size and shape of hydrometeor and calculate the horizontal and vertical velocity according to the particle exposure location in the image and interval time, the detailed specifications of the PMCS is shown in Table 1.

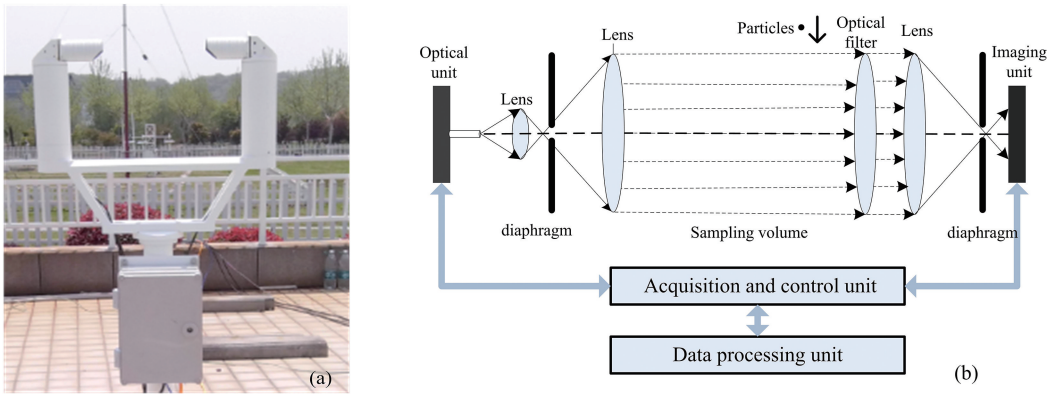

Fig. 1 (a) A photograph of the PMCS deployed in NUIST (b) The schematic of PMCS measure principle

Table 1 Specifications of the PMCS

Wavelength: 460nm (Center Wavelength)	Power consumption: <1W
Work voltage: 12V	Temporal resolution: 1min
Image resolution: 640×480	Sampling frequency: 50fps
Sampling volume: 250mm (length) ×32mm (width) ×24mm (high)	Resolution: 0.1mm
Drop size range: 0mm ~ 7.1mm	Velocity range: 0m/s ~ 12m/s

3 Calibration scheme

3.1 Calibration experiment

The main part of ambient light is the visible light in the natural environment. The center wavelength of PMCS is 460 nm. Therefore, the ambient light may interfere the image and make the parallel light beam of PMCS have divergence angle, which would cause different shape of particles in the image under the different ambient light and location of the sampling space. There are 0.5 mm, 0.8 mm, 1.0 mm, 1.2 mm, 1.5 mm, 2.0 mm, 2.38 mm, 2.5 mm, 3.0 mm, 3.5 mm, 4.0 mm, 4.76 mm, 5.0 mm calibration spheres are used to carry out calibration experiments in sunny, cloudy, night conditions. They are placed is in the center location of sampling space and 5 complete images per diameter are obtained. There are 1.0 mm, 2.0 mm, 3.0 mm, 4.0 mm calibration spheres are used to carry out calibration experiments in D, DC, C, LC, L locations of sampling space in cloudy conditions and get 5 complete images per location. The detailed locations are shown in Fig 2.

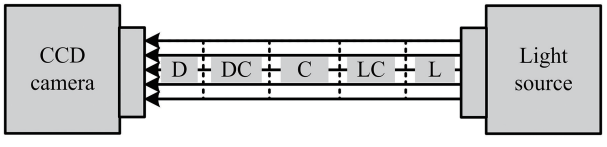

Fig. 2 The different locations of sampling space

3.2 Calibration algorithm

The core of the PMCS is a planar CCD image sensor, but the CCD has the characteristics of pixel non-uniformity, voltage instability, light refraction, reflection, scattering and absorption, which would cause noise and defocusing blur in the image (Fig. 3a). As shown in Fig.3, the image processing can be divided into 5 steps as follows: in step 1, it extract valid particle according to the pixels 4-connected principle; in step2, a median filter algorithm is used to remove the noise, in step 3 and 4, the point spread function and erosion are applied to restore the filtered images respectively; at last an appropriate threshold is selected to obtain the binary images.

However, the influence of divergence angle and ambient light to the original images is higher in the field observation than in the laboratory. To address this issue, we need to calibrate the instrument again and optimize the image processing. Now, we assume the radius of median filtering is $r1$, the radius of point spread function (PSF) is $r2$, the radius of erosion is $r3$, and the binary threshold is *thresh* which can be defined as:

$$thresh = I/I_{max}$$

Where the I is the brightness of image and the I_{max} is the max value of I. In the meantime, the axis ratio b/a and equivolumetric diameter D_{eq} are used to quantify the shape of drops in the images. The axis ratio and equivolumetric diameter of the calibration sphere is 1 and D_0 respectively. Hence the object of image processing can be defined as:

$$\min U = \left[\alpha\left|1 - b/a\right| + (1\text{-}\alpha)\left|\frac{D_{eq} - D_0}{D_0}\right|\right]$$

Where U is the object value, α is weight factor, a is the long axis, b is the short axis, $D_{eq} = (a^2 \cdot b)^{-1/3}$.

The image features [13] represent the characteristics of gray image. The signification and formula of them are shown in Table 2, where the $F(I)$ is image gray level histogram. All of them are calculated by the image gray level histogram. These image features could be applied in the calibration scheme that based on the relationship between image features and image processing parameters.

Summarizing the above analysis, we can design the calibration algorithm, as shown in Fig4. Firstly, the calibration algorithm exacts the valid images from the original images. Secondly, the image features are calculated from valid images and the optimized parameters of image processing are obtained from optimized processing with enumeration method where all the range of $r1$, $r2$, $r3$ are $[3,5,7,9]$ pixels and the range of the *thresh* is from 0.0001 to 1. Then, the relationship between optimized parameters and image features can be determined. At last, the calibration scheme could be checked by the other calibration images.

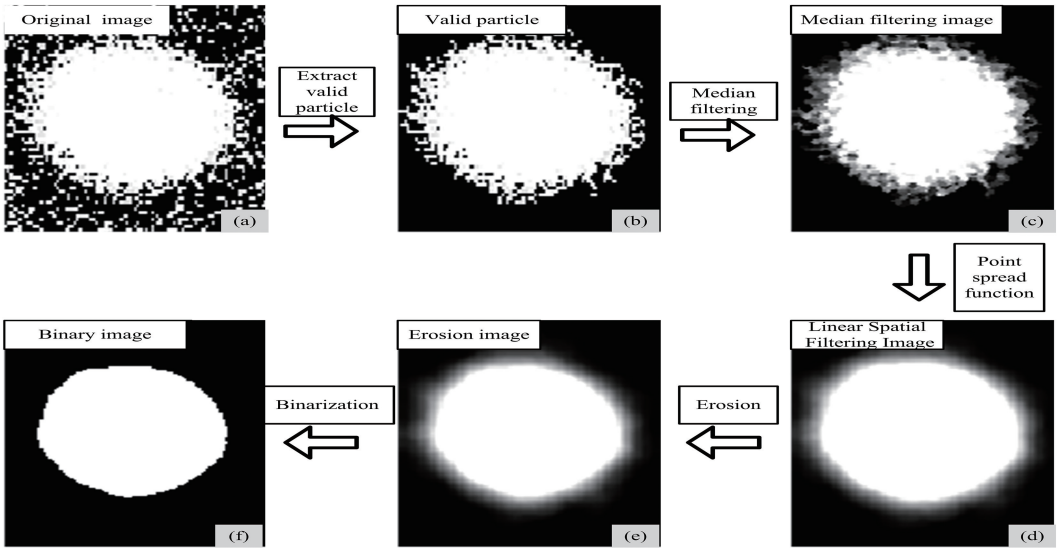

Fig. 3 Flowchart of the PMCS image processing

Table 2 The signification and formula of image features

Image Features	Notation	Formula	Signification
Probability density function	$f(I)$	$f(I) = F(I) / \sum_{I=0}^{255} F(I)$	The probability density function of image gray level histogram.
Total brightness value	I_0	$I_0 = \sum_{I=0}^{255} F(I) \cdot I$	The summation of image brightness values.
Mean brightness value	μ_I	$\mu_I = \sum_{I=0}^{255} f(I) \cdot I$	The average values of image brightness values.
Standard deviation	σ_I	$\sigma_I{}^2 = \sum_{I=0}^{255} f(I) \cdot (I - \mu_I)^2$	The standard deviation of image brightness values.
Fractional standard deviation	FSD	$FSD = \sigma_I / \mu_I$	The fractional standard deviation of image gray level histogram.
Particle area	$Area$	$Area = \sum_{I=1}^{255} F(I)$	The number of pixel which the brightness value>0.

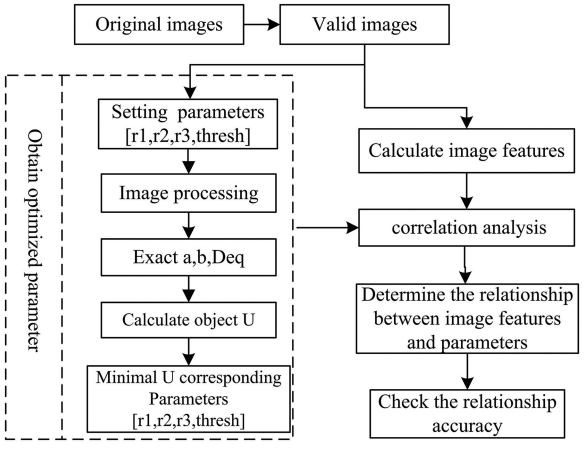

Fig. 4 Flowchart of the calibration algorithm

4 Calibration results

4.1 The influence of location and ambient light on the images

There are 932 sample images had been obtained in the location experiment, and 2116 sample images had been obtained in the ambient light experiment. We can use one half of them to analyze the calibration processing, and other half of them to check the reliability of the images processing parameters after calibration. The mean brightness value μ_I can reflect the shadowing level by particles, and the particle area *Area* can reflect the size of the shadowing area by particles. Both of them can be used to analyze the influence of location and ambient light on the images.

The influence of location on the images are depicted in Fig.5. The calibration spheres with diameters of 1cm, 2cm, 3cm, and 4cm have similar characteristics. For the same particle, the mean brightness value μ_I decreases with the increasing distance of particle to the Light source (Fig.5a-d). The main reason for this is that the closer the particles to the Light source, the more ambient light would be integrated into in the CCD sensor, especially at D and L location. However, for the same particle, the particle area *Area* increases as the distance of particle to the Light source increases (Fig.5e-5h). The reason for this maybe that the light of PMCS have divergence. Moreover, μ_I and *Area* have negative correlation with location for the same particle, that maybe due to the influence by the light diffraction, refraction, reflection and so on.

The influence of ambient light on the images are depicted in Fig.6. The mean brightness value μ_I increases with the diameter no matter in the sunny, cloudy and night conditions (Fig.6a), and the average μ_I of sunny is minimum among the three conditions in every diameter. The particle area *Area* increases with diameters in all conditions too. But, there are no significant diversities among the three conditions. The reason for the phenomenon is that the ambient light could affect the fixed exposure brightness but could not affect the shadow level in the CCD sensor.

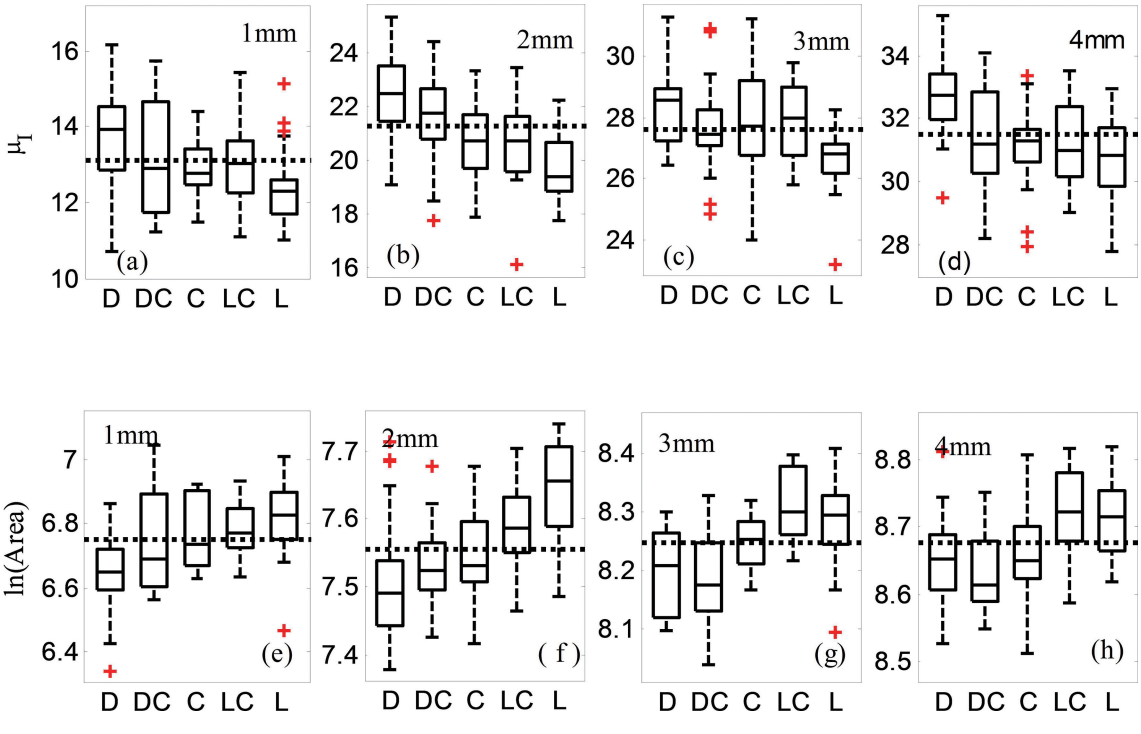

Fig. 5 The influence by the location for same particle

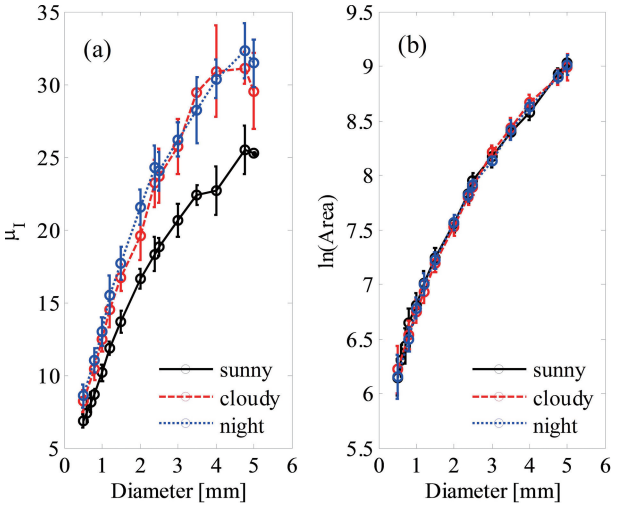

Fig. 6 The influenceof the ambient light for different particles in diameter

4.2 Determine the images processing parameters

To determine the image processing parameters, 1524 sample images had been addressed by the calibration algorithm, the results are shown in the Table 3. There are 49.46% of images have selected 3 pixels as radium for median filtering , and 8 9 . 5 1 % of all images have chosen 3 pixels as radium for erosion. As for the radium of PSF modeling, [3, 5, 7, 9] have been chosen with similar probability and the 7 pixels mode has highest probability 27.84%. In fact, all the three image processings model can not completely diminish the blur in images. Therefore, selecting an appropriate *thresh* for binarization is the key process, which determine whether the real particle could be obtained or not.

The *thresh* has strong negative correlation with diameter D, mean brightness μ_I , standard deviation σ_I and particle area *Area*, all of their correlation coefficients are above 0.8, as shown in the Table 4. In the meantime, the strong correlation were also existed among the different image features. For example, the correlation coefficient between μ_I and Area is 0.9375, which due to that all of these image features are calculated from image gray level histogram. This phenomenon maybe imply that all of these image features have similar characteristics, we can debate the relationship between one of them with *thresh*.

Table 3 Percentage of radium were selected for different image processing

Image processing	Radius	3	5	7	9
Median filtering	r_1	49.46%	19.49%	14.88%	16.17%
PSF modeling	r_2	24.63%	21.09%	27.84%	26.45%
Erosion	r_3	89.51%	6.32%	2.36%	1.82%

Table 4 The correlation coefficient among different image features

	D	*thresh*	I_0	μ_I	σ_I	*FSD*	*Area*
D	1.0000	-0.8493	0.9090	0.9082	0.7879	-0.8772	0.9744
thresh	-0.8493	1.0000	-0.6434	-0.8647	-0.8372	0.8090	-0.8807
I_0	0.9090	-0.6434	1.0000	0.8362	0.7004	-0.7543	0.8863
μ_I	0.9082	-0.8647	0.8362	1.0000	0.9592	-0.8067	0.9357
σ_I	0.7879	-0.8372	0.7004	0.9592	1.0000	-0.6410	0.8362
FSD	-0.8772	0.8090	-0.7543	-0.8067	-0.6410	1.0000	-0.9115
Area	0.9744	-0.8807	0.8863	0.9357	0.8362	-0.9115	1.0000

In general, the *Area* can't be influenced by ambient light and it is sensitive to the variety of sampling locations. Moreover, it has strongest correlation with *thresh*, which correlation coefficient is -0.8807. Hence, the *Area* could be used to establish function relationship with *thresh*. The results are shown in the Fig. 7. The scatter points of *Area* and *thresh* have a negative exponent trend, the linear least square fitting method could be used to retrieve *Area -thresh* relationship, the result as shown in following formula which the RMSE is 0.0762 and the R^2 is 0.8988.

$$thresh = (0.0025Area + 0.04746)^{-1} + 0.2242$$

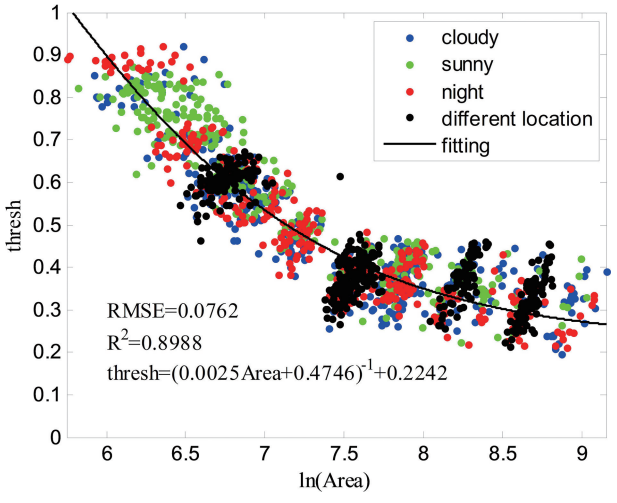

Fig. 7 The relationship between *thresh* and *Area*

4.3 Validation of the calibration

In the new image processing scheme, the radius of median filtering is set as 3 pixels, the radius of PSF modeling is 7 pixels, the erosion is taken as 3 pixels, and the binary thresh is obtained from the *Area -thresh* relationship according to the results of our new calibration scheme. The rest of 1524 sampling images were used to examine the validation of the new scheme. Then the results of the new and traditional calibration methods are compared with each other, as shown in Fig.8, in which the $< \varepsilon >$ represents the average errors and the σ represents the standard deviation. From Fig. 8a, both of the new and traditional schemes could get equivolumetric diameters which are accordance with real diameters. Whereas, the equivolumetric diameters of new scheme have less variation than traditional one in the same diameter range. The $< \varepsilon >$ of new scheme's equivolumetric diameters is 0.041 mm and the σ is 0.115 mm, but the $< \varepsilon >$ of traditional scheme's equivolumetric diameters is 0.077 mm and the σ is 0.17 mm. The result of the axis ratios are shown in Fig 8b, in which the shadow region represents the axis ratio measured range with a 0.17 mm quantization size error. For example, a 0.5 mm ball can register a diameter in the range 0.33 ~ 0.67 mm, hence measured axis ratio may lie in the range 0.33/0.67 ~ 0.67/0.33. From the Fig.8b, the spread around the average axis ratios of the two scheme are within the expected bounds. Moreover, the average axis ratios of new scheme are more consistent with the real one. The $< \varepsilon >$ of new scheme's axis ratio is 0.011 and the σ is 0.085. The $< \varepsilon >$ of traditional one is 0.019 and the σ is 0.092. It can be seen that the new calibration scheme have smaller average errors and standard deviation in the measurement of eqivolumetric diameters and axis ratios than traditional scheme, indicating that the *Area -thresh* relationship can help to adjust the binary threshold and reduce the influence to the image by external factors such as the ambient light, CCD pixel non-uniformity and the divergence of parallel light beam on the measurement of paticles. Therefore, the new scheme could do better than the traditional scheme in the calibration of PMCS.

5 Field measurements

A PMCS was located at Nanjing, and a rainfall on 17 June 2015 has been observed, in which 159882 images of raindrops were recorded. All of these images were addressed by the new image processing scheme, the PMCS after calibration performance well. The observed axis ratio was consistent with the empirical relationship by Beard [14], as shown in Fig.9a. A comparison of drop size distribution (DSD) has been made among PMCS measure-

ments before calibration, PMCS measurements after calibration and OTT measurements, as shown in Fig. 9b. The DSD (D>0.625) observed by PMCS after calibration is more consistent with OTT than before calibration. The trend of Rain Accumulation observed by PMCS and OTT were consistent with the rain gauge (Fig. 9c). And the Rain Accumulation calculated by the PMCS before calibration and after calibration, OTT, rain gauge were 44.3652 mm, 45.2732 mm, 48.6135 mm, and 46.700 mm, respectively. Choosing the rain gauge as a reference, the relative error of PMCS after calibration is -3.06% and before calibration is -5%.

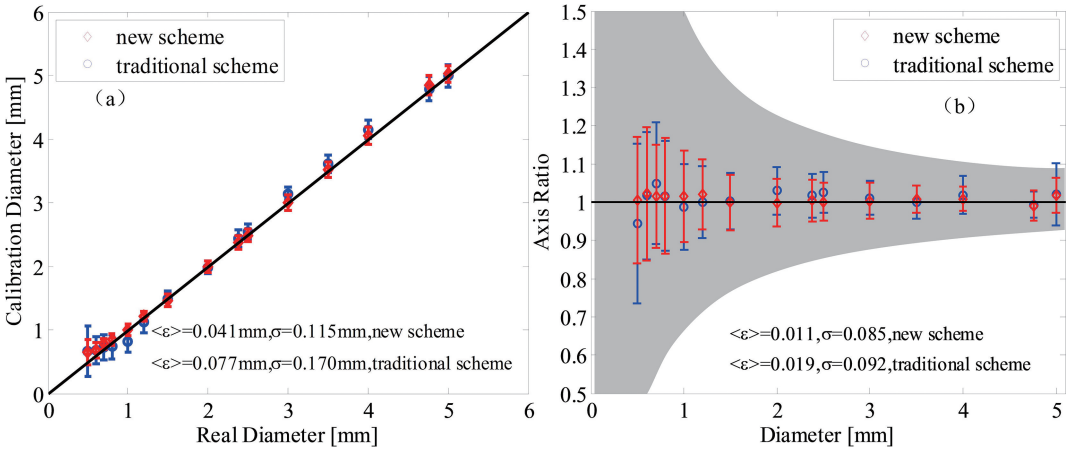

Fig. 8 The equivolumetric diameter and axis ratio for calibration sphere in different diameter

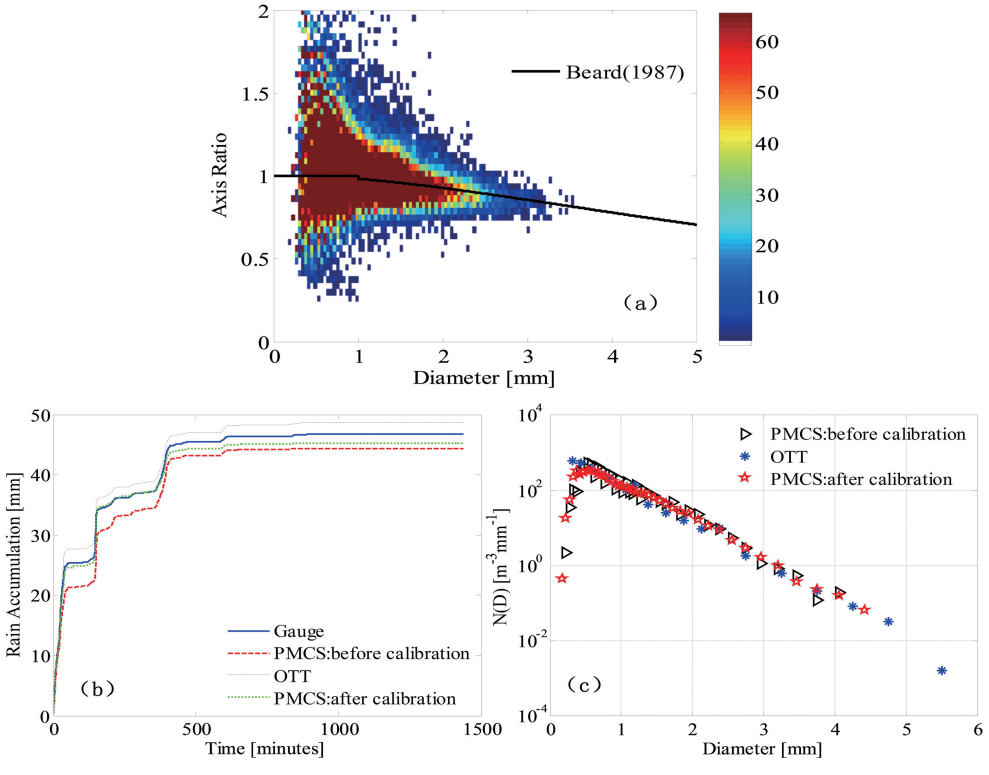

Fig. 9 (a) The axis ratio distribution were calculated by the new image processing scheme; (b) The average DSD observed by PMCS before and after calibration and OTT (c) The Rain Accumulation observed by different kinds of instrument.

6 Conclusions

In order to diminish the effect of the ambient light and CCD pixel non-uniformity to the Precipitation Micro-physical Characteristics Sensor. A modified calibration scheme was designed and calibration experiments in sunny, cloudy, night, different location of sample space were carried out. The conclusion is shown as following:

1) The different locations of sample space can affect both of the mean brightness and the particle area. With the distance to the light source increasing, the mean brightness decreases and the particle area increases. The different ambient light can affect the mean brightness of images but can't affect the particle area of images. The binary thresh has strong correlation with image features, especially the particle area which correlation coefficient is -0.8807.

2) The new image processing scheme could deal with the image calibration well, the average errors of equivolumetric diameter was 0.041 mm, the standard deviation was 0.115 mm and the average errors of the axis ratio was 0.011, the standard deviation was 0.085.

3) In the field measurement, the new image processing scheme performance well, too. The observed axis ratio was consistent with the empirical relationship by Beard. The DSD ($D>0.625$) which observed by PMCS after calibration was more consistent with OTT than before calibration. The relative error of rain accumulation was -3.06% after calibration which had improved 1.94% to the initial one.

Acknowledgment

We thank professor HUANG Xingyou of NUSIT for his continued and highly support of this work in the field measurement. And this work is supported by the National Natural Science Foundation of China (grant no 41327003, 41475020 and 41505135).

References

[1] LIU X, GAO T, LIU L, et al. Advances in Micro-physical Features and Measurement Techniques ofRaindrops[J]. Advances in Earth Science, 2013, 28(11):1217-1226.

[2] JOSS J, WALDVOGEL A.Ein Spektrograph für Niederschlagstropfen mit automatischer Auswertung [J]. Pure & Applied Geophysics, 1967, 68(68):240-246.

[3] MANGM L, JOSS J. An optical distrometer for measuring size and velocity of hydrometeors [J]. Journal of Atmospheric and Oceanic Technology, 2000(17): 130-139.

[4] BARTHAZY E, GOKE S, SCHEFOLD R, et al. An optical array instrument for shape and fall velocity measurements of hydrometeors [J]. Journal of Atmospheric and Oceanic Technology, 2004(21): 1400-1416.

[5] KRUGER A. Two-Dimensional Video Disdrometer: A Description [J]. Journal of Atmospheric & Oceanic Technology, 2002, 19(5):602-617.

[6] NEWMAN A J, KUCERA P A, BLIVEN L F. Presenting the Snowflake Video Imager (SVI)[J]. Journal of Atmospheric & Oceanic Technology, 2009, 26(2):167.

[7] LIU X C, GAO T C, LIU L. A Video Precipitaion Sensor for Imaging and Velocimetry of Hydrometeors [J]. Atmos. Meas. Tech., 2014, 7:2037-2046.

[8] LIU X C, GAO T C, LIU L, et al. Research on microphysical property of raindrops based on particle imaging velocimetry technology [J]. Acta Phys. Sin., 2014.63(2):029203-1-029203-7.

[9] LIU X C, GAO T C, LIU L, et al. Research on microphysical property of snowfall based on particle imageing velocimetry technology [J]. Acta Phys. Sin., 2014.63(19):199201-1-199201-9.

[10] LIU X C. Research on Measurement Technology and Application of Precipitation Micro-physical Characteristics [D]. Ningjing: PLA University of Science and Technology,2014:25-35.

[11] HUANG F ZHANG D. Study of Optical Rainfall Sensing Method [D]. Kunming: Kunming university of science and technology, 2014:16-45.

[12] GAO T C, SU X Y, YANG S C, et al. Calibration method for automatic optical measurement instrument of precipitation based on linear CCD [J]. Journal of PLA University of Science and Technology (Natural Science Edition), 2013.14(3):315-321.

[13] GONZALEZ R C, WINTZ P. Digital image process-

ing.[J]. Prentice Hall International, 2001, 28(4): 484 - 486.

[14] BEARD K V, CHUANG C. A New Model for the Equilibrium Shape of Raindrops.[J]. Journal of the Atmospheric Sciences, 1987, 44:1509-1524.

Authors' Biographies

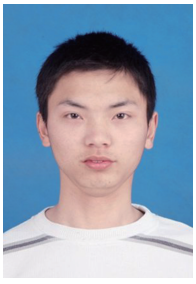

SHU Xiaojian, was born in Sichuan province, China on October, 1990. He received his B. Sc. degree in NUIST of China. Now he is a master degree candidate in PLA University of Science and Technology. His main research interest is ground-based meteorological observation techniques.

E-mail: 734675624@qq.com

GAO Taichang, was born in Shanxi province, China on November, 1958. He received his B. Sc. degree in 1982 from College of Air Force Meteorology. Currently, he is a Professor in PLA University of Science and Technology. His main research interest is atmospheric sounding theory and technique.

E-mail: 2009gaotc@gmail.com

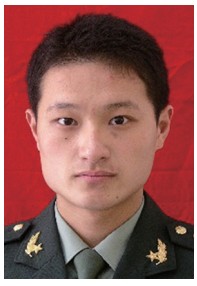

LIU Xichuan, was born in Hebei province, China on December, 1985. He received his B. Sc. Degree, M. Sc. Degree and Ph. D. Degree in 2006, 2010, 2014 from PLA University of Science and Technology. Now he is an instructor in PLA University of Science and Technology. His main research interest is atmospheric remote sensing and atmospheric sounding.

HU Shuai, was born in Jiangxi province, China on July, 1990. He received his B. Sc. degree in 2012 from PLA University of Science and Technology. Now he is a doctor´s degree candidate in PLA University of Science and Technology. His main research interest is atmospheric remote sensing and atmospheric sounding.